Molecular Astrophysics 6 (2017) 47–58

Contents lists available at ScienceDirect

Molecular Astrophysics

journal homepage: www.elsevier.com/locate/molap

Inelastic cross sections and rate coefficients for collisions between CO and H_2

Christina Castro[a], Kyle Doan[a], Michael Klemka[a], Robert C. Forrey[a,*], Benhui Yang[b], Phillip C. Stancil[b], N. Balakrishnan[c]

[a] Department of Physics, Penn State University, Berks Campus, Reading, PA 19610-6009, United States
[b] Department of Physics and Astronomy and the Center for Simulational Physics, University of Georgia, Athens, Georgia 30602, United States
[c] Department of Chemistry, University of Nevada, Las Vegas, NV 89154, United States

ARTICLE INFO

Article history:
Received 22 November 2016
Revised 20 January 2017
Accepted 21 January 2017
Available online 23 January 2017

Keywords:
Molecular data
Molecular collisions
Carbon monoxide
Hydrogen

ABSTRACT

A five-dimensional coupled states (5D-CS) approximation is used to compute cross sections and rate coefficients for CO+H_2 collisions. The 5D-CS calculations are benchmarked against accurate six-dimensional close-coupling (6D-CC) calculations for transitions between low-lying rovibrational states. Good agreement between the two formulations is found for collision energies greater than 10 cm^{-1}. The 5D-CS approximation is then used to compute two separate databases which include highly excited states of CO that are beyond the practical limitations of the 6D-CC method. The first database assumes an internally frozen H_2 molecule and allows rovibrational transitions for $v \leq 5$ and $j \leq 30$, where v and j are the vibrational and rotational quantum numbers of the initial state of the CO molecule. The second database allows H_2 rotational transitions for initial CO states with $v \leq 5$ and $j \leq 10$. The two databases are in good agreement with each other for transitions that are common to both basis sets. Together they provide data for astrophysical models which were previously unavailable.

1. Introduction

H_2 and CO are the most abundant molecules in most astrophysical environments and have been the focus of numerous astrophysical studies and observations (van Dishoeck and Black, 1998). CO is easily excited by collisions with H_2 and other species in interstellar gas, and the resulting emission lines are commonly used to provide important diagnostics of gas density and temperature. When these environments are irradiated with an intense UV field, the radiation drives the chemistry and internal level populations out of equilibrium. Models which aim to interpret the emission lines arising from these environments must account for all mechanisms which can excite or de-excite the molecules. Simulation packages have been developed (Petit et al., 2006; Rollig, 2007; Shaw et al., 2005; Warin et al., 1996) which account for inelastic transitions of both H_2 and CO in various astrophysical environments such as photodissociation regions (PDRs) which occur between hot HII (ionized hydrogen) and cold molecular regions. Observations of star-forming regions and protoplanetary disks (PPDs) of young stellar objects have shown evidence of rovibrational transitions involving states of CO which are highly excited. In particular, vibrational transitions have been detected in the near infrared by the *Infrared Space Observatory*, the Gemini Observatory, and the Very Large Telescope (VLT). A recent VLT survey (Brown et al., 2013) of 69 PPDs found that 77% of the sources showed CO vibrational bands, including vibrational level v as high as 4 and rotational level j as high as 32. CO vibrational bands in the 1–5 μm regime will soon be accessible by NASA's *James Webb Space Telescope* which will allow the warm inner regions of young stellar objects to be probed. To reliably model these environments requires an extensive set of state-to-state rate coefficients for rovibrational transitions induced by H_2 collisions. Many of these rate coefficients are either unavailable or else are estimated with potentially unreliable methods (Walker et al., 2014).

To provide accurate data for astrophysical models generally requires a large and concerted effort between several communities within atomic and molecular physics. Experimental data are sparse but are critical for benchmarking theoretical methods (Costes and Naulin, 2016; Faure et al., 2016; Yang et al., 2015). Numerical solution of the Schrödinger equation offers the best hope for generating the bulk of the needed data. However, to make these computations possible, it is often necessary to invoke decoupling approximations which reduce the dimensionality of the full scattering problem. Even when full-dimensional quantum dynamics

* Corresponding author.
E-mail address: rcf6@psu.edu (R.C. Forrey).

http://dx.doi.org/10.1016/j.molap.2017.01.003
2405-6758/

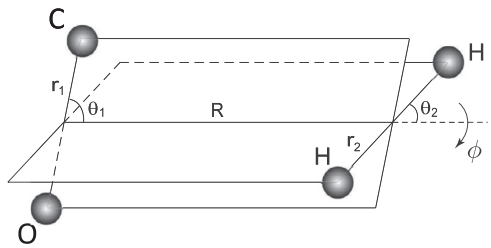

Fig. 1. Six-dimensional Jacobi coordinates for CO-H_2. R is the distance between the centers of mass of CO and H_2, r_1 and r_2 are bond lengths, θ_1 and θ_2 are the respective angles between $\vec{R}$ and $\vec{r}_1$ and $\vec{r}_2$, and ϕ is the dihedral or twist angle.

calculations are feasible, their accuracy depends on the underlying electronic structure calculations and potential energy surface (PES) which is used as input. Recently, a high-level full-dimensional PES was developed for CO+H_2 and used in a six-dimensional close-coupling (6D-CC) formulation (Yang et al., 2015) which is essentially an exact treatment of the dynamics. The calculations were in excellent agreement with experiment for vibrational de-excitation of CO, whereas prior calculations which consisted of various levels of approximation varied by more than two orders of magnitude (Bacic et al., 1985a; 1985b; Flower, 2012; Reid et al., 1997). Subsequently, the 6D-CC approach was used to provide additional high-quality cross sections for CO+H_2 collisions (Yang et al., 2016). These calculations are computationally demanding and have been completed for only a small subset of rovibrational levels needed for the astrophysical models. Nevertheless, these calculations provide the best benchmarks for transitions where experimental data are lacking, and may serve as a foundation for testing approximate schemes which aim to further extend the available data. One such scheme is the coupled states or centrifugal sudden (CS) approximation which requires significantly less computational effort due to the decoupling of orbital and internal angular momenta. A recent study (Forrey et al., 2015) compared 6D-CS and 6D-CC cross sections for CO+H_2 and found encouraging results for energies above 10 cm^{-1}. Additional decoupling of the "twist" angle between the two molecules led to a 5D-CS approximation which also yielded encouraging results. In the present work, we compute a large database of cross sections and rate coefficients using the 5D-CS approximation. The 5D-CS calculations are compared with existing 6D-CC results in order to assess the expected level of accuracy of the approximation. The database provides a balance between accuracy and computational efficiency and is made available in a convenient format for use in astrophysical models.

2. Theory

The quantum mechanical CC and CS formulations for diatom-diatom collisions have been given previously (Alexander and DePristo, 1977; Green, 1975; Heil et al., 1978). In order to clarify the differences between the 5D and 6D formulations, we provide a brief summary of the theory. The Hamiltonian of the four-atom system may be written

$$H(\vec{r}_1,\vec{r}_2,\vec{R}) = T(\vec{r}_1) + T(\vec{r}_2) + T(\vec{R}) + V(\vec{r}_1,\vec{r}_2,\vec{R}), \tag{1}$$

where $T(\vec{R})$ is a radial kinetic energy term describing the center-of-mass motion, $T(\vec{r}_1)$ and $T(\vec{r}_2)$ are kinetic energy terms for the diatomic molecules, and $V(\vec{r}_1,\vec{r}_2,\vec{R})$ is the potential energy of the system. It is convenient to define

$$V(\vec{r}_1,\vec{r}_2,\vec{R}) = U(\vec{r}_1,\vec{r}_2,\vec{R}) + V(\vec{r}_1) + V(\vec{r}_2), \tag{2}$$

where $V(\vec{r}_1)$ and $V(\vec{r}_2)$ are the two-body potential energies of the isolated CO and H_2 molecules, and $U(\vec{r}_1,\vec{r}_2,\vec{R})$ is the four-body interaction potential which vanishes at large separations. The 6D

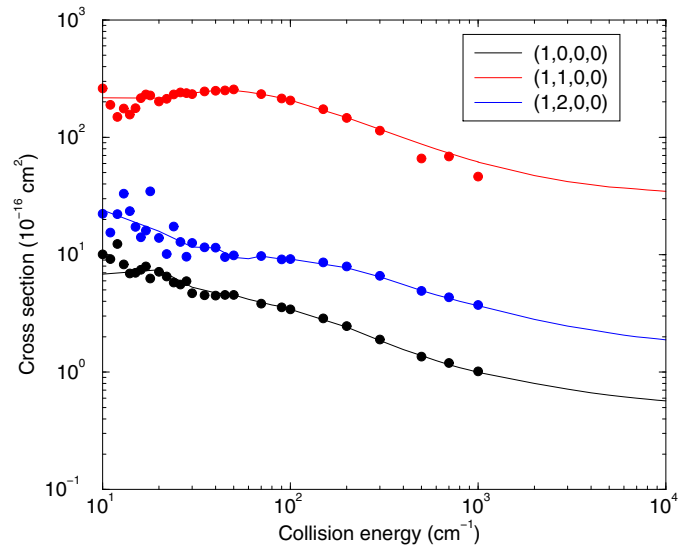

Fig. 2. Elastic and rotationally inelastic cross sections for inital state (1, 1, 0, 0). Solid lines are 5D-CS results and points are 6D-CC results (Yang et al., 2016).

Jacobi coordinate system in Fig. 1 is used where R is the distance between the centers-of-mass of the diatomic molecules, θ_1 is the angle between $\vec{r}_1$ and $\vec{R}$, θ_2 is the angle between $\vec{r}_2$ and $\vec{R}$, and ϕ is the out-of-plane dihedral angle or "twist" angle. The interaction potential may be expanded as

$$U(\vec{r}_1,\vec{r}_2,\vec{R}) = \sum_{all\ \lambda} A_{\lambda_1,\lambda_2,\lambda_{12}}(r_1,r_2,R)\, Y_{\lambda_1,\lambda_2,\lambda_{12}}(\hat{r}_1,\hat{r}_2,\hat{R}) \tag{3}$$

with

$$Y_{\lambda_1,\lambda_2,\lambda_{12}}(\hat{r}_1,\hat{r}_2,\hat{R}) = \sum_{all\ m} \langle \lambda_1 m_{\lambda_1} \lambda_2 m_{\lambda_2} | \lambda_{12} m_{\lambda_{12}} \rangle\, Y_{\lambda_1 m_{\lambda_1}}(\hat{r}_1) \times Y_{\lambda_2 m_{\lambda_2}}(\hat{r}_2)\, Y^*_{\lambda_{12} m_{\lambda_{12}}}(\hat{R}), \tag{4}$$

where $\langle \ldots | \ldots \rangle$ represents a Clebsch–Gordan coefficient and $Y_{\lambda m}(\hat{r})$ is a spherical harmonic. The total wave function for the four-atom system is expanded in terms of a diabatic basis set which contains products of molecular wave functions $\chi_{v_i j_i}(r_i)$ with vibrational and rotational quantum numbers v_i and j_i, respectively. We describe the combined molecular state (CMS) comprised of CO(v_1, j_1) and H_2(v_2, j_2) using the notation $n = (v_1, j_1, v_2, j_2)$ so that the basis functions for vibrational motion may be written

$$\chi_n(r_1,r_2) = \chi_{v_1 j_1}(r_1)\chi_{v_2 j_2}(r_2)\ . \tag{5}$$

The rotational wave functions are given in terms of products of spherical harmonics in a total angular momentum representation. The basis sets are defined by the number of vibrational levels and the maximum rotational level $j_v^{\max}$ for a given v. The radial interaction potential matrix elements are obtained by integrating over the internal coordinates

$$B^{\lambda_1,\lambda_2,\lambda_{12}}_{n;n'}(R) = \int_0^\infty \int_0^\infty \chi_n(r_1,r_2) A_{\lambda_1,\lambda_2,\lambda_{12}}(r_1,r_2,R) \times \chi_{n'}(r_1,r_2) r_1^2 r_2^2 dr_1 dr_2. \tag{6}$$

The full potential matrix depends on the scattering formulation. For the CC method, the channels are defined by the set {n, j_{12}, l}, where l is the orbital angular momentum quantum number

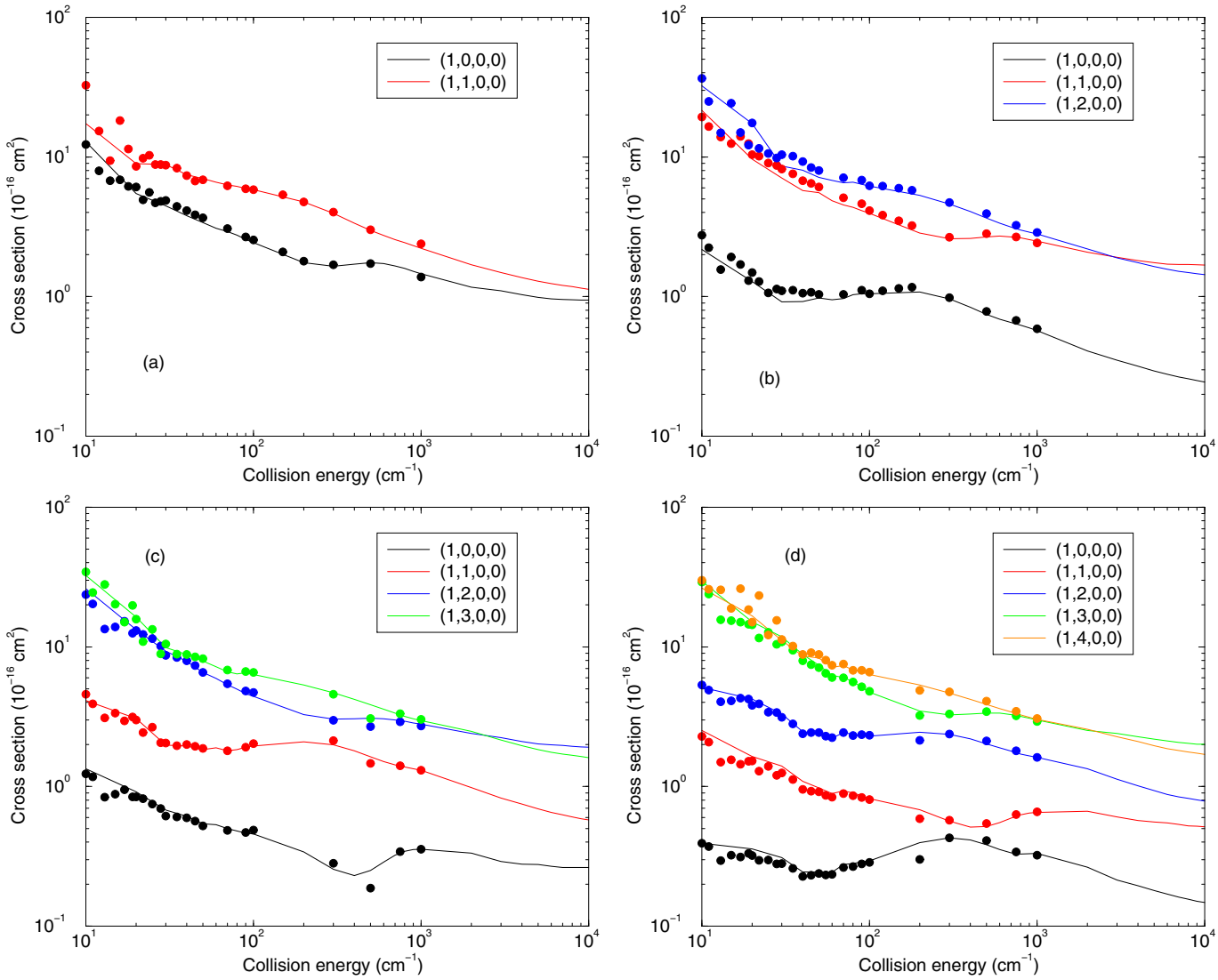

Fig. 3. Rotationally inelastic cross sections for transitions between the initial state (a) (1, 2, 0, 0), (b) (1, 3, 0, 0), (c) (1, 4, 0, 0), (d) (1, 5, 0, 0) and the final state indicated. Solid lines are 5D-CS results and points are 6D-CC results (Yang et al., 2016).

and $\vec{j}_{12} = \vec{j}_1 + \vec{j}_2$. The total angular momentum quantum number J is defined by $\vec{J} = \vec{l} + \vec{j}_{12}$, and the interaction potential matrix for 6D-dynamics is given by

$$U^{J}_{n j_{12} l; n' j'_{12} l'}(R) = (4\pi)^{-3/2} \sum_{all\ \lambda} (-1)^{j'_1+j'_2+j_{12}+J}$$
$$\times \left([j_1][j_2][j_{12}][l][j'_1][j'_2][j'_{12}][l'][\lambda_1][\lambda_2][\lambda_{12}]^2\right)^{1/2}$$
$$\times \begin{pmatrix} l' & \lambda_{12} & l \\ 0 & 0 & 0 \end{pmatrix} \begin{pmatrix} j'_1 & \lambda_1 & j_1 \\ 0 & 0 & 0 \end{pmatrix} \begin{pmatrix} j'_2 & \lambda_2 & j_2 \\ 0 & 0 & 0 \end{pmatrix}$$
$$\times \begin{Bmatrix} l & l' & \lambda_{12} \\ j'_{12} & j_{12} & J \end{Bmatrix} \begin{Bmatrix} j_{12} & j_2 & j_1 \\ j'_{12} & j'_2 & j'_1 \\ \lambda_{12} & \lambda_2 & \lambda_1 \end{Bmatrix} B^{\lambda_1,\lambda_2,\lambda_{12}}_{n;n'}(R) \tag{7}$$

which is diagonal with respect to J and independent of the projection of $\vec{J}$ in the space-fixed frame. The notations (===), {===}, and {≡ ≡ ≡} are the usual 3j, 6j, and 9j symbols, and $[j] = (2j+1)$. For the 5D-CS formulation, the potential matrix is given by

$$U^{m_1,m_2}_{n;n'}(R) = (4\pi)^{-3/2} \sum_{all\ \lambda} (-1)^{\lambda_1+\lambda_2+m_1+m_2}$$
$$\times \left([j_1][j_2][j'_1][j'_2][\lambda_1][\lambda_2][\lambda_{12}]^2\right)^{1/2}$$
$$\times \begin{pmatrix} j'_1 & \lambda_1 & j_1 \\ 0 & 0 & 0 \end{pmatrix} \begin{pmatrix} j'_2 & \lambda_2 & j_2 \\ 0 & 0 & 0 \end{pmatrix} \begin{pmatrix} j'_1 & \lambda_1 & j_1 \\ -m_1 & 0 & m_1 \end{pmatrix}$$
$$\times \begin{pmatrix} j'_2 & \lambda_2 & j_2 \\ -m_2 & 0 & m_2 \end{pmatrix} \begin{pmatrix} \lambda_1 & \lambda_2 & \lambda_{12} \\ 0 & 0 & 0 \end{pmatrix} B^{\lambda_1,\lambda_2,\lambda_{12}}_{n;n'}(R) \tag{8}$$

which is diagonal with respect to m_1 and m_2, the projection quantum numbers of $\vec{j}_1$ and $\vec{j}_2$, respectively. The 5D-CS formulation averages the twist-angle dependence of the PES and yields a potential matrix which is independent of j_{12}. Both dynamical formulations require the solution of a set of coupled radial equations derived from the Schrödinger equation. Cross sections may

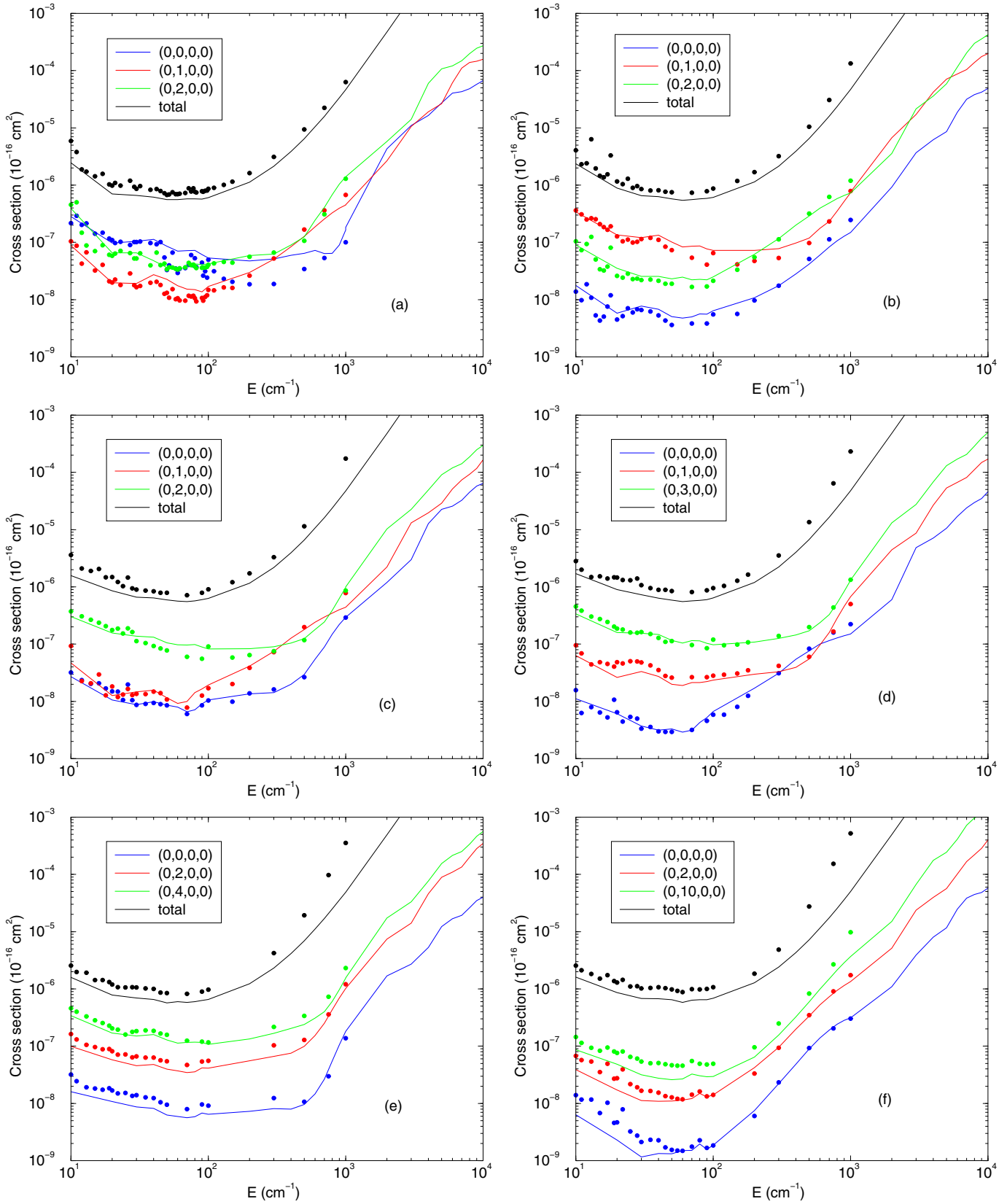

Fig. 4. Vibrationally inelastic cross sections for transitions between the initial state (a) (1, 0, 0, 0), (b) (1, 1, 0, 0), (c) (1, 2, 0, 0), (d) (1, 3, 0, 0) (e) (1, 4, 0, 0), (f) (1, 5, 0, 0) and the final state indicated. Solid lines are 5D-CS results and points are 6D-CC results (Yang et al., 2016).

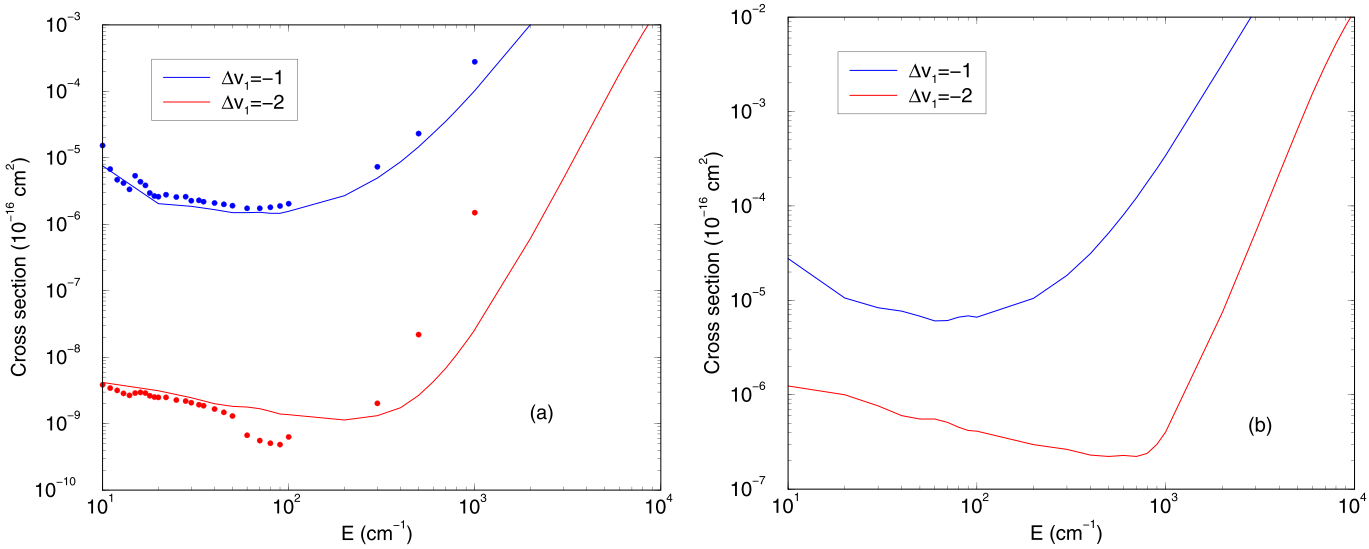

Fig. 5. Vibrational quenching cross sections for (a) (2, 0, 0, 0) and (b) (5, 0, 0, 0) initial states. Solid lines are 5D-CS results and points are 6D-CC results (Yang et al., 2016). The $\Delta v_1 = -2$ transitions are at least one order of magnitude smaller than $\Delta v_1 = -1$ transitions for both sets of calculations.

be expressed in terms of the appropriate T-matrix by

$$\sigma^{\text{6D-CC}}_{n\to n'}(E_c) = \frac{\pi}{(2j_1+1)(2j_2+1)2\mu E_c} \times \sum_{j_{12}j'_{12}ll'J} (2J+1) \left| T^J_{nj_{12}l;n'j'_{12}l'}(E_c) \right|^2 , \quad (9)$$

and

$$\sigma^{\text{5D-CS}}_{n\to n'}(E_c) = \frac{\pi}{(2j_1+1)(2j_2+1)2\mu E_c} \times \sum_{\bar{l}m_1m_2} (2\bar{l}+1) \left| T^{\bar{l}m_1m_2}_{n;n'}(E_c) \right|^2 , \quad (10)$$

where E_c is the collision energy, and μ is the reduced mass of the CO-H_2 system. The CS approximation assumes the off-diagonal Coriolis matrix elements of $\hat{l}^2$ with respect to m_1 and m_2 may be neglected, and the diagonal elements may be approximated by an effective orbital angular momentum quantum number $\bar{l}$ which replaces l. For all calculations in the present work, $\bar{l} \equiv J$ which is its average value between $|J - j_{12}|$ and $J + j_{12}$. Rate coefficients may be obtained by thermally averaging the cross sections over a Maxwellian velocity distribution

$$k_{n\to n'}(T) = \sqrt{\frac{8k_BT}{\pi\mu}}(k_BT)^{-2} \int_0^\infty \sigma_{n\to n'}(E_c)\, e^{-E_c/k_BT} E_c\, dE_c , \quad (11)$$

where T is the temperature and k_B is Boltzmann's constant.

3. Results

All calculations use the 6D PES reported previously (Yang et al., 2015) which is currently the only available full-dimensional surface that is flexible enough to handle vibrational transitions for both molecules. This surface yielded 6D-CC results for vibrational relaxation of CO which were in excellent agreement with experiment, whereas prior calculations consisting of various dynamical decoupling approximations varied by more than two orders of magnitude (Bacic et al., 1985a; 1985b; Flower, 2012; Reid et al., 1997). It should be noted that the 6D PES (Yang et al., 2015) has been shown to be less accurate than the V12 PES (Jankowski et al., 2013) for calculating pure rotational cross sections at very low energies (Faure et al., 2016; Yang et al., 2016). However, these energies do not play a significant role in determining the rate coefficients over the temperature range considered in the present work. Therefore, we consider the 6D-CC calculations on the 6D PES to be a suitable benchmark for calibrating the 5D-CS calculations described here.

Previous work (Forrey et al., 2015) showed that 5D-CS and 6D-CS results for CO+H_2 were virtually identical for collision energies above 10 cm^{-1}. The agreement with 6D-CC calculations was also found to be good at these energies for the limited amount of data that was available for comparison. Recently, new 6D-CC results have been reported (Yang et al., 2016) which allow for more extensive testing of the 5D-CS approximation. All calculations in the present work were performed using a modified version of the TwoBC code (Krems, 2006) which replaces Eqs. (7) and (9) with Eqs. (8) and (10). The radial coordinates of both molecules were represented as discrete variables with 20 points each. Gauss–Legendre quadratures were used for θ_1 and θ_2 with 14 points each, and a Chebyshev quadrature was used for ϕ with 8 points. The maximum values for λ_1 and λ_2 were 10 and 6, respectively. The log-derivative matrix propagation method (Johnson, 1973; Manolopoulos, 1986) was used to integrate the set of coupled equations derived from the Schrödinger equation from $R = 4 - 18$ a.u. in steps of 0.05 a.u. The calculations were performed in unit steps for four decades of collision energy on a logarithmic energy grid. The maximum effective orbital angular momentum for each set of calculations is given by

$$\bar{l}_{max} = \begin{cases} 20, & E_c = 1 - 10 \text{ cm}^{-1} , \\ 40, & E_c = 10 - 100 \text{ cm}^{-1} , \\ 80, & E_c = 100 - 1,000 \text{ cm}^{-1} , \\ 160, & E_c = 1,000 - 10,000 \text{ cm}^{-1} . \end{cases} \quad (12)$$

Excellent agreement was seen at the E_c boundaries, and convergence tests at low E_c verified that the results were converged to within 5% or better with respect to size of the basis set.

The 5D-CS calculations were performed for collision energies between 10 and 10,000 cm^{-1} and compared against 6D-CC results obtained previously (Yang et al., 2016). Fig. 2 shows elastic and rotationally inelastic cross sections for the (1, 1, 0, 0) initial state. The curves for rotational excitation (1, 2, 0, 0) and de-excitation

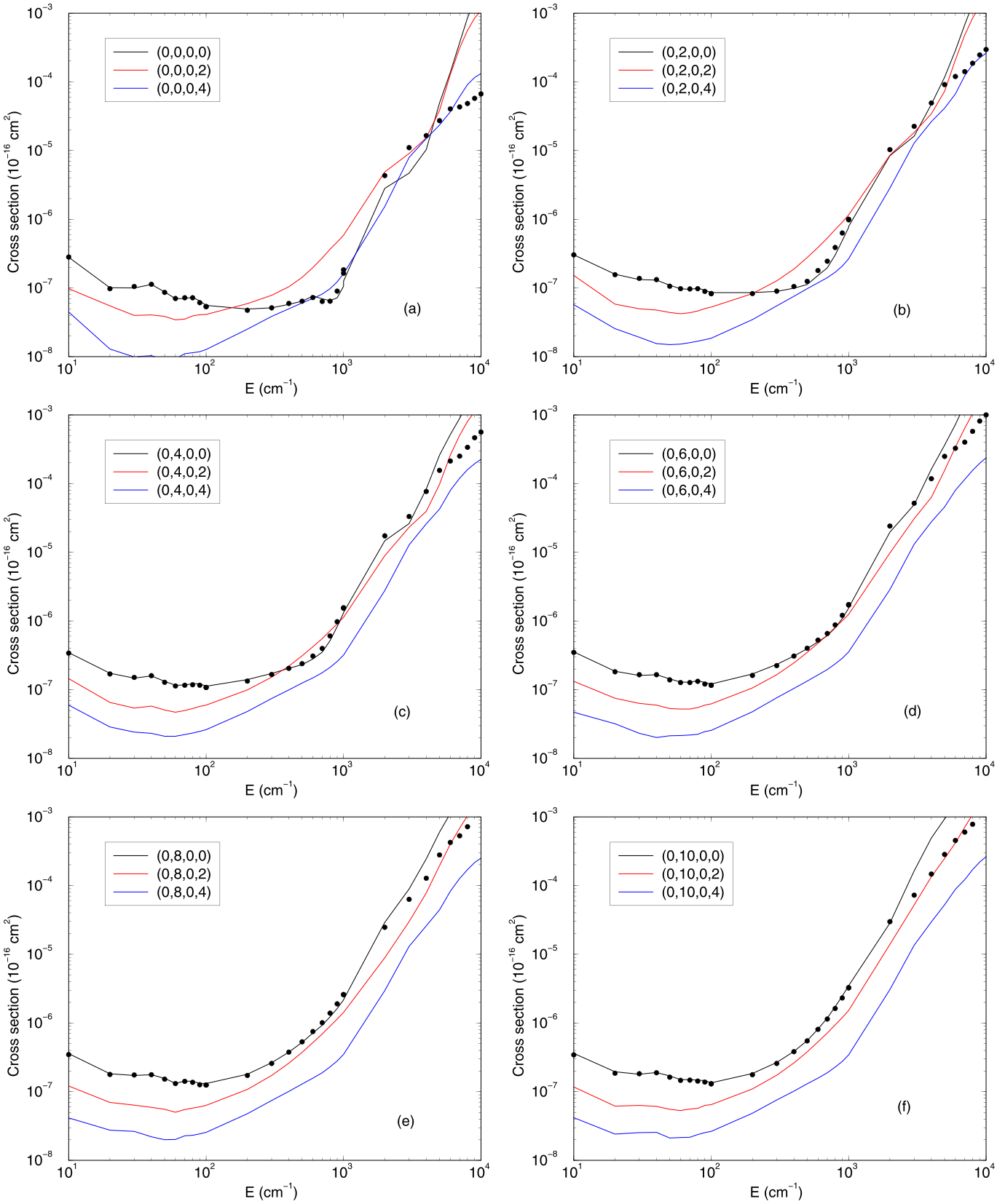

Fig. 6. Vibrationally inelastic cross sections for transitions between the initial state (a) (1, 0, 0, 0), (b) (1, 2, 0, 0), (c) (1, 4, 0, 0), (d) (1, 6, 0, 0) (e) (1, 8, 0, 0), (f) (1, 10, 0, 0) and the final state indicated. Solid lines are 5D-CS results which allow H_2 rotational transitions and points are 5D-CS results which restrict H_2 to be in the ground rovibrational state.

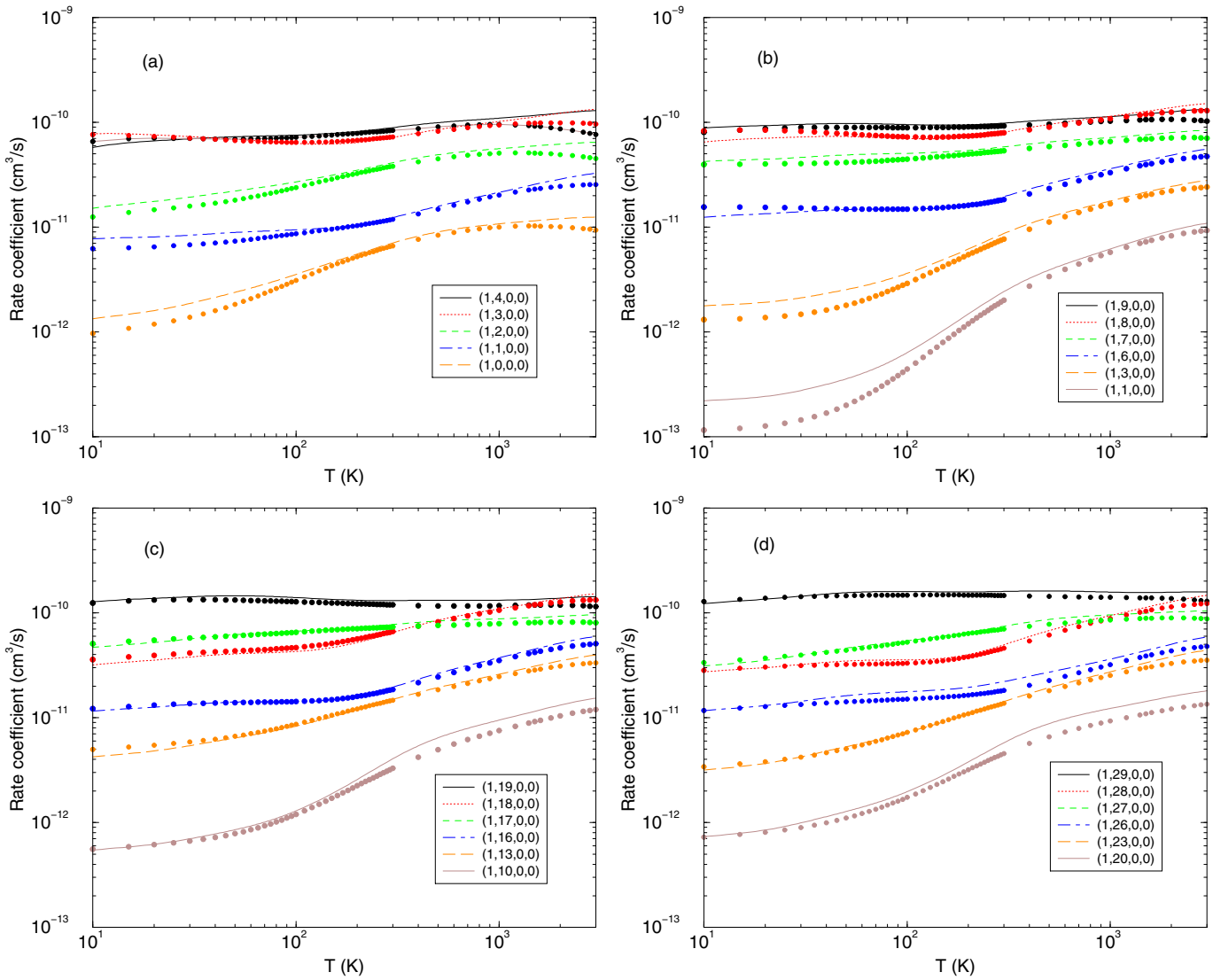

Fig. 7. Rate coefficients for rotational transitions from initial state (a) (1, 5, 0, 0), (b) (1, 10, 0, 0), (c) (1, 20, 0, 0) and (d) (1, 30, 0, 0). Also shown (colored points) are rigid rotor results reported previously (Yang et al., 2010) for (0, j_1, 0, 0). (For interpretation of the references to colour in this figure legend, the reader is referred to the web version of this article.)

(1, 0, 0, 0) are in near perfect agreement with the corresponding 6D-CC points for energies above 100 cm^{-1}. The agreement remains good for energies down to 10 cm^{-1}, however, the 5D-CS results do not show the resonant structure that was found in the 6D-CC calculations. This is partly due to the energy step size, which is too large to resolve the resonances, however, it is not expected that the effective $\bar{l}$ used in the CS calculations would accurately describe the resonances even if a finer energy grid were used. The elastic (1, 1, 0, 0) cross section shows a similar pattern of agreement with the exception of small discrepancies at 500 and 1000 cm^{-1}. This is probably due to incomplete convergence of the 6D-CC elastic cross section with respect to higher partial waves.

Fig. 3 shows a set of similar comparisons for the (1, 2, 0, 0), (1, 3, 0, 0), (1, 4, 0, 0), and (1, 5, 0, 0) initial states. Only the rotational de-excitation cross sections are shown. The agreement between the 5D-CS and 6D-CC results is again very good for energies between 10 and 1000 cm^{-1}. Apart from a few small discrepancies, the approximate 5D-CS formulation is able to reproduce the results of the 6D-CC calculation and extend them to higher energies. The agreement is not quite as good for the vibrationally inelastic cross sections shown in Fig. 4. Cross sections for transitions from the same initial states as Figs. 2 and 3 are shown for selected final states. The total cross section represents the sum over all final CO rotational level contributions in the $v_1 = 0$ manifold. The state-to-state cross sections show a larger number of discrepancies between the 5D-CS and 6D-CC calculations. However, these discrepancies are generally small, and the 5D-CS results are able to provide a good approximation to the overall shape and relative magnitudes of the state-to-state cross sections for vibrationally inelastic collisions. The agreement between the two computational methods for the total cross section appears to worsen at high energies as the initial rotational level of the CO molecule increases. This is due to the contributions from transitions to high rotational levels. For example, the (1, 5, 0, 0) to (0, 10, 0, 0) cross section in Fig. 4(f) shows a relatively large discrepancy compared to the (0, 0, 0, 0) and (0, 2, 0, 0) cross sections which are in very good agreement at high energies. This pattern was found for all of the vibrationally inelastic cross sections and may be attributed to basis set truncation error in the 6D-CC calculations which used

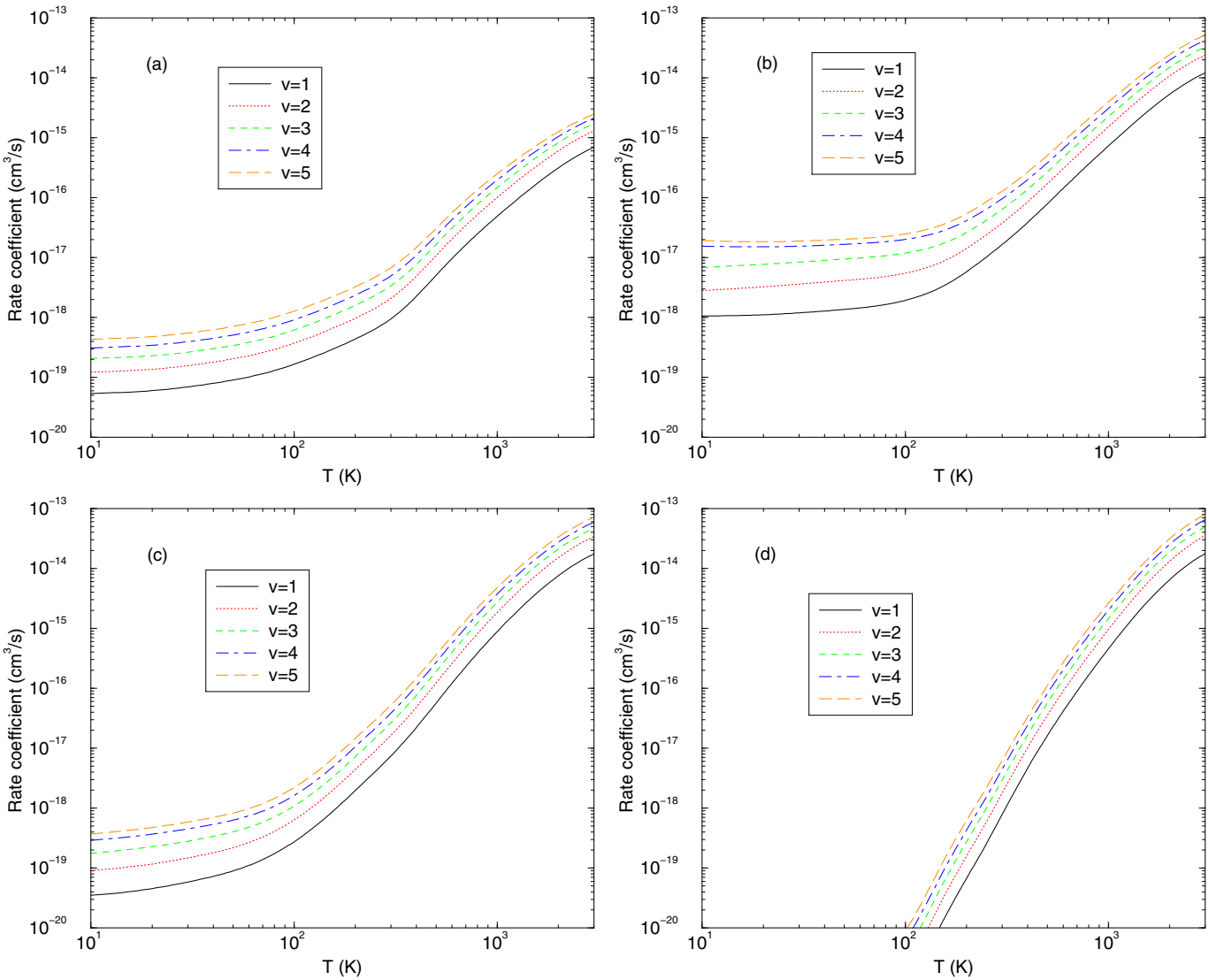

Fig. 8. Rate coefficients for transitions from $(v, 10, 0, 0)$ to (a) $(v-1, 0, 0, 0)$, (b) $(v-1, 10, 0, 0)$, (c) $(v-1, 20, 0, 0)$, and (d) $(v-1, 30, 0, 0)$ obtained from the "frozen-H_2" basis set.

$j^{max}_{v_1=0} = 22$ and $j^{max}_{v_1=1} = 20$. These limits provide good convergence for vibrationally inelastic cross sections involving low-lying rotational levels at all energies. However, for transitions involving high rotational levels, the truncation limits are insufficient, particularly at high collision energies. It should be noted that the truncation in the 6D-CC calculations was a necessity due to the computational resource limitations. For comparison, the 5D-CS calculations in Figs. 2–4 used $j^{max}_{v_1=0} = j^{max}_{v_1=1} = 40$.

The size of the CO vibrational basis set is considered in Fig. 5. For both the 5D-CS and 6D-CC calculations, the vibrational basis set included $v_1 = 0-2$. The vibrational quenching cross section for the (2, 0, 0, 0) initial state is dominated by the $\Delta v_1 = -1$ contribution, and the comparison between the 5D-CS and 6D-CC results is similar to the (1, 0, 0, 0) initial state shown in Fig. 4. The $\Delta v_1 = -2$ contribution is at least two orders of magnitude smaller than the $\Delta v_1 = -1$ contribution for both sets of calculations at the energies shown. The agreement between the 5D-CS and 6D-CC results is not as good for the $\Delta v_1 = -2$ contribution above 300 cm^{-1}, but given the relatively small magnitude of this cross section, the discrepancy is not very significant. Expanding the basis set to include closed vibrational levels yielded no change to these results. Fig. 5(b) shows similar results for the (5, 0, 0, 0) initial state. These cross sections are again dominated by the $\Delta v_1 = -1$ contribution, however, the $\Delta v_1 = -2$ contribution increases relative to the $\Delta v_1 = -1$ contribution due to the decreasing difference between vibrational energy levels. The small contribution from $\Delta v_1 = -2$ transitions allows a compact representation of the vibrational motion to be obtained using basis sets with v_1 equal to v and $v-1$, where v is the vibrational level of the initial state. This enables large rotational basis sets to be employed (see Table 1).

The size of the para-H_2 rotational basis set is considered in Fig. 6. The solid curves correspond to a rotational basis set which includes $j_2 = 0-4$. In order to improve the computational efficiency of these calculations, the truncation limit $j^{max}_{v_1=1}$ of the initial CO rotational basis was reduced to 20. The figure shows that the cross sections for vibrational relaxation of CO accompanied by rotational excitation of H_2 are comparable in magnitude to those with no change in H_2. Expanding the H_2 basis further to allow more rotational excitation yielded small contributions and

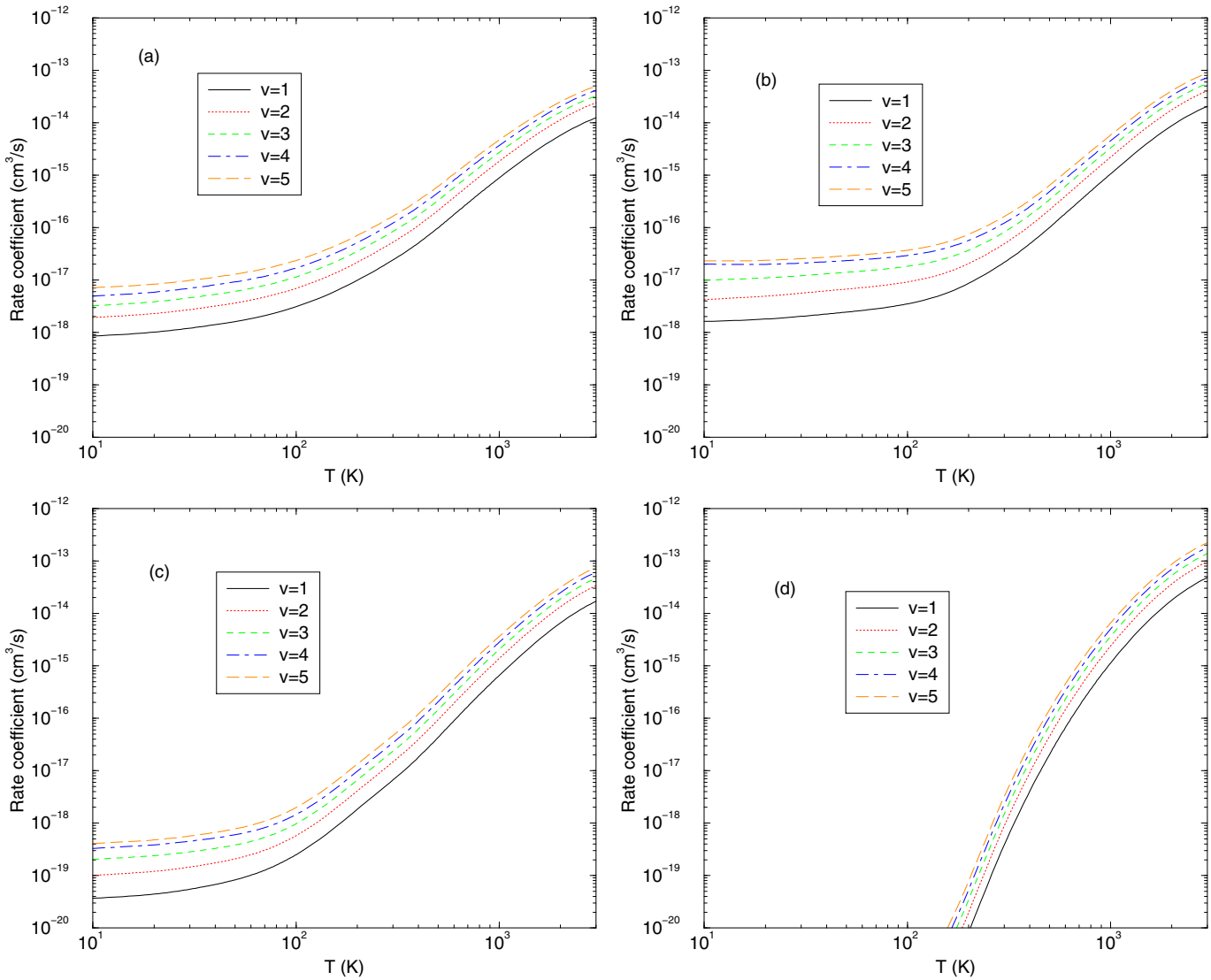

Fig. 9. Rate coefficients for transitions from $(v, 20, 0, 0)$ to (a) $(v-1, 10, 0, 0)$, (b) $(v-1, 20, 0, 0)$, (c) $(v-1, 30, 0, 0)$, and (d) $(v-1, 40, 0, 0)$ obtained from the "frozen-H_2" basis set.

Table 1
Basis set parameters used for the databases.

Basis set	v	j_v^{max}	j_{v-1}^{max}	j_{v-2}^{max}	j_1	j_2	j'_1	j'_2
frozen-H_2	0	40	–	–	0–30	0, 1	0–40	0, 1
	1	40	40	–	0–30	0, 1	0–40	0, 1
	2	40	40	40	0–20	0, 1	0–40	0, 1
	3–5	40	40	–	0–20	0, 1	0–40	0, 1
flexible-H_2	0	20	–	–	0–10	0, 1	0–20	0–4, 1–5
	1–2	20	40	–	0–10	0, 1	0–40	0–4, 1–5
	3–5	20	40	–	0–10	0	0–40	0–4

provided little change to these results. The points shown in the figure correspond to the $j_{v_1}^{max} = 40$ basis set with H_2 restricted to its ground rovibrational state. The agreement in the $H_2(0, 0)$ cross sections is nearly perfect for the two sets of calculations for energies below 2000 cm^{-1}. At higher energies, it is not clear which basis set yields the more reliable result due to the different truncation limits on H_2 and CO.

In order to explore rovibrational transitions for a large sample of internal states and collision energies, we constructed two separate databases for state-to-state cross sections and rate coefficients. The "frozen H_2" database uses $j_v^{max} = 40$ and includes transitions for initial CO$(j_1 = 0 - 30)$ due to collisions with rovibrationally rigid para-$H_2(j_2 = 0)$ and ortho-$H_2(j_2 = 1)$. The "flexible H_2" database uses $j_v^{max} = 20$ and includes transitions for

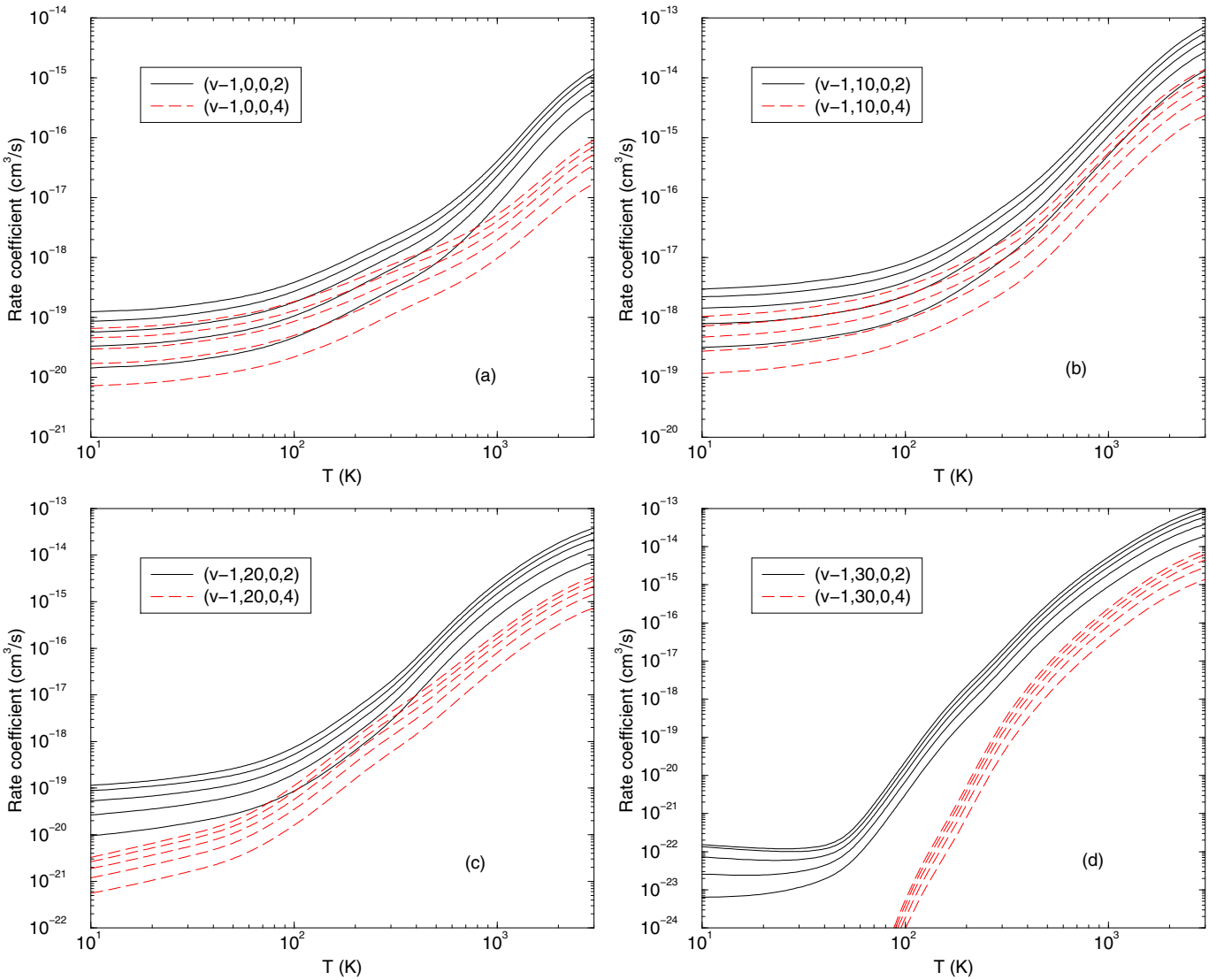

Fig. 10. Rate coefficients for transitions from (v, 10, 0, 0) to (a) ($v-1, 0, 0, j$), (b) ($v-1, 10, 0, j$), (c) ($v-1, 20, 0, j$), and (d) ($v-1, 30, 0, j$) obtained from the "flexible-H_2" basis set. The solid black curves correspond to H_2(0, 2) final states, and the dashed red curves to H_2(0, 4) final states. Both sets of curves increase uniformly with v for $v = 1-5$. (For interpretation of the references to colour in this figure legend, the reader is referred to the web version of this article.)

initial CO($j_1 = 0-10$) due to collisions with rotationally flexible para-H_2($j_2 = 0, 2, 4$) and ortho-H_2($j_2 = 1, 3, 5$). Additional details of the basis sets are given in Table 1.

Figs. 7–9 show rate coefficients for a sample of initial states from the frozen-H_2 database. The pure rotational relaxation rate coefficients in Fig. 7 are very similar to the rigid rotor results reported previously (Yang et al., 2010). The present results are for $v = 1$, however, similar plots for higher v are nearly identical, which confirms the validity of the rigid rotor approximation for pure rotational transitions of CO. For the rovibrationally inelastic transitions shown in Figs. 8 and 9, the curves are well-ordered with respect to the initial vibrational level and generally exhibit a step-like structure with increasing temperature. The height of the steps increases with final state rotational level j_1', and the rate coefficients are found to be relatively large for j_1' near the basis set truncation limit at the highest temperatures shown. This indicates that the rovibrationally inelastic calculations are still not fully converged at the highest temperatures ($T > 1000$ K) even with the large truncation limit $j_{v-1}^{\max} = 40$.

Fig. 10 shows results from the flexible-H_2 database for the (v, 10, 0, 0) initial state. Rate coefficients for transitions involving no change in H_2 are nearly identical to those presented in Fig. 8 and are not shown. Vibrational relaxation of CO($v = 1-5$) for transitions which leave H_2 in a rotationally excited state yield rate coefficients which are well-ordered with respect to v as shown. The solid black and dashed red curves represent $\Delta j_2 = 2$ and $\Delta j_2 = 4$ transitions for H_2, respectively, with both sets of curves increasing with v. The step-like structure is again seen in the rate coefficients and is a general feature for both databases.

The databases include CO collisions with both para-H_2 and ortho-H_2. Fig. 11 shows the ratio of total CO vibrational quenching rate coefficient for ortho-H_2 and para-H_2 collisions for several initial states of CO. The ratio is generally found to approach unity for $T > 100$ K. As the initial rotational level of CO is increased, the ratio is close to unity for all vibrational levels and temperatures shown. These results suggest that para-H_2 rate coefficients may be directly used for ortho-H_2 rate coefficients for $T > 100$ K

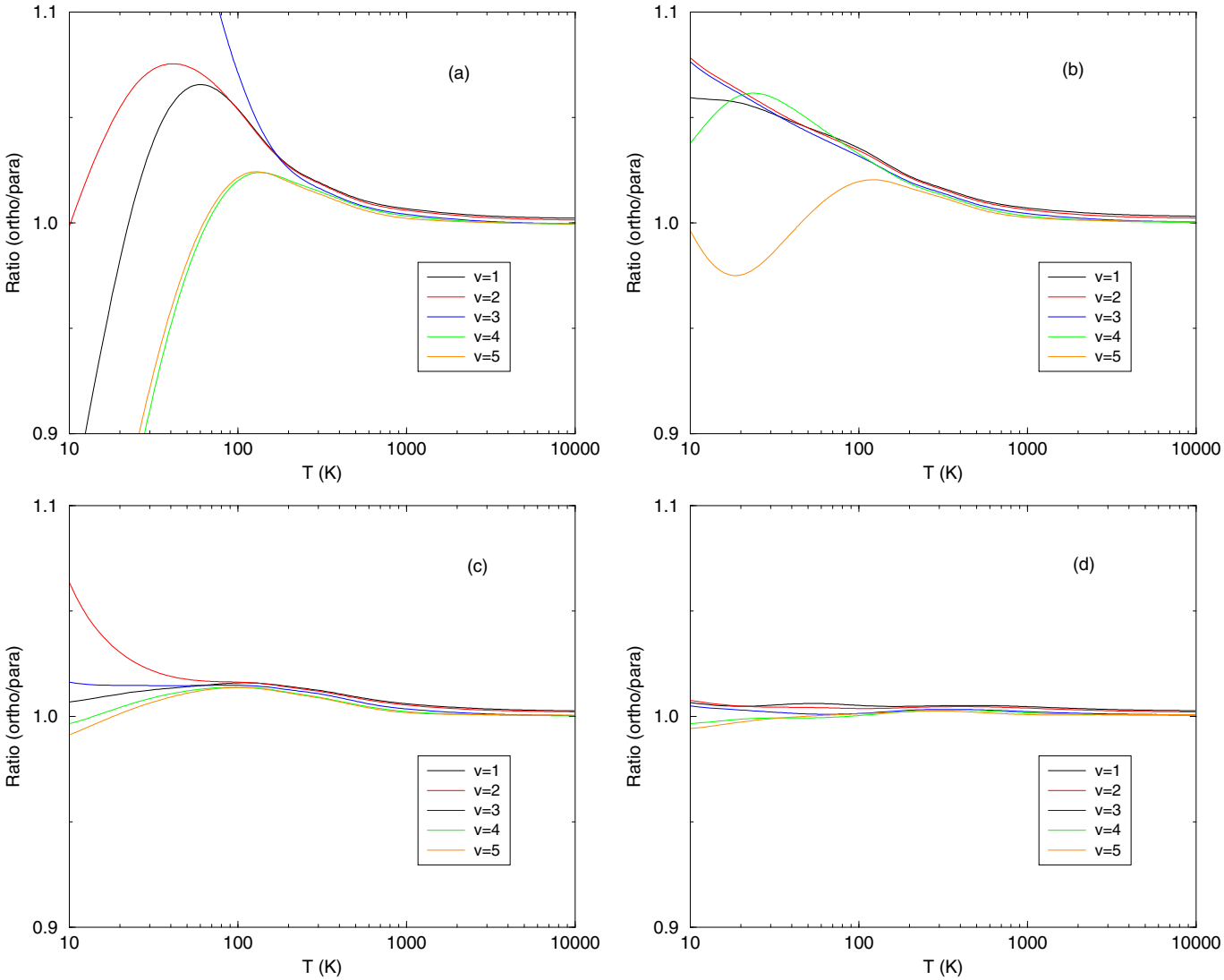

Fig. 11. Ratio of vibrational quenching rate coefficients for collision with ortho-H_2 and para-H_2. The panels correspond to CO in the initial state (a) (v, 0), (b) (v, 5), (c) (v, 10), and (d) (v, 20) making a transition to the final state ($v-1$) summed over all final rotational levels.

with an error of no more than 10% and a considerable savings in computational expense.

4. Conclusions

Full-dimensional dynamics of CO interacting with H_2 is a challenging computational problem for quantum mechanical scattering formulations. The closely spaced rotational levels for CO lead to substantial internal angular momentum coupling between the molecules. When orbital angular momentum is properly taken into account within the numerically exact CC formulation, the additional angular momentum coupling creates a bottleneck for many rovibrationally excited initial states, which makes it impossible to bring the calculations to completion on a practical timescale. In such cases, it is necessary to use approximate methods to obtain the desired data. The CS approximation offers a good compromise between accuracy and computational effort. In this approximation, the exact orbital angular momentum quantum number is replaced by an effective value, and the off-diagonal Coriolis coupling between states with different projection quantum numbers is neglected. Averaging the PES over the twist angle to obtain the 5D-CS approximation further improves the computational efficiency without introducing a significant additional loss of accuracy beyond the CS approximation itself.

Using the 5D-CS approximation, we constructed two separate databases for state-to-state cross sections and rate coefficients for CO+H_2 collisions. The "frozen-H_2" database assumes the collision takes place with the H_2 molecule frozen in the lowest rotational level of a given symmetry. This restriction allows the bulk of the computational effort to be used for the CO basis sets which include $j_v^{\max} = j_{v-1}^{\max} = 40$ for each initial v. The database then includes transitions for each basis set with initial CO($v = 0-5$, $j = 0-30$). The "flexible-H_2" database allows rotational excitation of H_2 during the collision. To compensate for the enlarged H_2 basis sets, the CO basis sets are reduced to $j_v^{\max} = 20$ with $j_{v-1}^{\max} = 40$, and a smaller set of transitions from initial CO($v = 0-5$, $j = 0-10$) is included in the database. The two databases are in good agreement with each other for transitions that are common to both basis sets. Both databases generally contain cross sections and rate coefficients for $E_c = 1-10,000$ cm^{-1} and $T = 10-3,000$ K. It would be desirable to improve the databases by replacing the 5D-CS cross sections with 6D-CC values for the lower energies, and by expanding the 5D-CS basis sets to include additional CO rotational levels at the higher energies. These extensions will be implemented

in future versions of the project. The present version provides a large amount of data which may be used as a starting point for further approximations (e.g. scaling) and provides important data for astrophysical models. Details of the databases are described in the supplementary material associated with this article. The databases may be downloaded from the UGA Excitation Database (http://www.physast.uga.edu/amdbs/excitation/) or PSU website (physics.bk.psu.edu/sigma/index.html).

We note that while the databases have enlarged the amount of collisional data available for CO+H_2, they nevertheless remain incomplete in the sense that all data between levels that are not included in the basis sets are assumed to be zero. These missing transitions are generally inefficient compared to the dominant allowed transitions, however, their omission could have an effect on radiative transfer calculations which require collisional data between all levels. In such applications, it may be necessary to merge the two databases and expand them further to include additional rotational and vibrational transitions.

Acknowledgments

This work was supported at Penn State by NSF Grant No. PHY-1503615, at UGA by NASA grant NNX12AF42G, and at UNLV by NSF Grant No. PHY-1505557.

Supplementary material

Supplementary material associated with this article can be found, in the online version, at 10.1016/j.molap.2017.01.003.

References

Alexander, M.H., DePristo, A.E., 1977. J. Chem. Phys 66, 2166.
Bacic, Z., Schinke, R., Diercksen, G.H.F., 1985. J. Chem. Phys. 82, 236.
Bacic, Z., Schinke, R., Diercksen, G.H.F., 1985. J. Chem. Phys. 82, 245.
Brown, J.M., et al., 2013. Astrophys. J. 770, 94.
Costes, M., Naulin, C., 2016. Chem. Sci. 7, 2462.
van Dishoeck, E.F., Black, J.H., 1998. Astrophys. J. 334, 771.
Faure, A., Jankowski, P., Stoecklin, T., Szalewicz, K., 2016. Sci. Rep. 6, 28449.
Flower, D.R., 2012. Mon. Not. R. Astron. Soc 425, 1350.
Forrey, R.C., Yang, B.H., Stancil, P.C., Balakrishnan, N., 2015. Chem. Phys. 462, 71.
Green, S., 1975. J. Chem. Phys. 62, 2271.
Heil, T.G., Green, S., Kouri, D.J., 1978. J. Chem. Phys. 68, 2562.
Jankowski, P., Surin, L.A., Potapov, A.V., Schlemmer, S., McKellar, A.R.W., Szalewicz, K., 2013. J. Chem. Phys. 138, 084307.
Johnson, B.R., 1973. J. Comp. Phys. 13, 445.
Krems, R.V., 2006. TwoBC – Quantum Scattering Program. University of British Columbia, Vancouver, Canada.
Manolopoulos, D.E., 1986. J. Chem. Phys 85, 6425.
Petit, F.L., Nehme, C., Bourlot, J.L., Roueff, E., 2006. Astrophys. J. Suppl. Ser. 164, 506.
Reid, J.P., Simpson, C.J.S.M., Quiney, H.M., 1997. J. Chem. Phys. 106, 4931.
Rollig, M., et al., 2007. A&A 467, 187.
Shaw, G., Ferland, G.J., Abel, N.P., Stancil, P.C., van Hoof, P.A.M., 2005. Astrophys. J. 624, 794.
Walker, K.M., Yang, B.H., Stancil, P.C., Balakrishnan, N., Forrey, R.C., 2014. Astrophys. J. 790, 96.
Warin, S., Benayoun, J.J., Viala, Y.P., 1996. A&A 308, 535.
Yang, B.H., Balakrishnan, N., Zhang, P., Wang, X., Bowman, J.M., Forrey, R.C., Stancil, P.C., 2016. J. Chem. Phys. 145, 034308.
Yang, B.H., Stancil, P.C., Balakrishnan, N., Forrey, R.C., 2010. Astrophys. J. 718, 1062.
Yang, B.H., Zhang, P., Wang, X., Stancil, P.C., Bowman, J.M., Balakrishnan, N., Forrey, R.C., 2015. Nat. Commun. 6, 6629.